

# The Magneto-Optical Voigt Parameter from Magneto-Optical Ellipsometry Data for Multilayer Samples with Single Ferromagnetic Layer

O. Maximova<sup>a, b, \*</sup>, S. Lyaschenko<sup>a</sup>, I. Tarasov<sup>a</sup>, I. Yakovlev<sup>a</sup>, Y. Mikhlin<sup>c</sup>,  
S. Varnakov<sup>a</sup>, and S. Ovchinnikov<sup>a, b</sup>

<sup>a</sup> Kirensky Institute of Physics, Siberian Branch, Russian Academy of Sciences, Krasnoyarsk, Russia

<sup>b</sup> Siberian Federal University, Krasnoyarsk, Russia

<sup>c</sup> Institute of Chemistry and Chemical Technology, Siberian Branch, Russian Academy of Sciences, Krasnoyarsk, Russia

\* e-mail: maximo.a@mail.ru

Received April 9, 2021; revised April 9, 2021; accepted April 19, 2021

**Abstract**—Calculations of the magneto-optical Voigt parameter  $Q$  were carried out using various models of reflecting media for thin films Fe|SiO<sub>2</sub>|Si(100) samples using the data of the in situ magneto-ellipsometry. The obtained spectral dependences of  $Q$  make it possible to choose the algorithm for the analysis of experimental magneto-ellipsometry data and demonstrate that magneto-optical parameter  $Q$  of iron is thickness-dependent.

**Keywords:** magneto-optical Voigt parameter, magneto-optical ellipsometry, data processing, ferromagnetic layers, optical models, refractive index, extinction coefficient

**DOI:** 10.1134/S1063783421090274

## 1. INTRODUCTION

In recent decades, much attention has been given to the synthesis and investigation of nanostructured materials with specified physical properties. The significant effect of surface atomic states on the macroscopic properties of the material as a whole is an important feature of such materials. Furthermore, continuous electronic devices miniaturization leads to the need for highly accurate prediction of their characteristics at various scales and under external influences. The development of surface investigation methods is required. Ultrahigh vacuum (UHV) analysis methods, which make it possible to study the atmosphere effect on the coatings properties, to control the chemical purity of the surface, as well as to simulate the conditions of outer space, high temperatures or temperature drops, are of great importance. Such methods are used in aerospace applications, in the catalysts production, functional coatings in electronics, etc. One of the selection criteria for these methods is the *in situ* implementation possibility, when both the synthesis and a detailed non-destructive analysis are carried out in one technological UHV chamber without the atmosphere impact on the sample.

Ellipsometry and magneto-modulated ellipsometry are exactly such methods that are convenient to be used *in situ*. Ellipsometry is a non-destructive investigation method with a high surface sensitivity. It is

widely used for spectral surface measurements of optical parameters that are necessary when optical filters, interference mirrors, optically active devices, solar panels, and various special coatings are developed [1]. Spectral measurements of the temperature dependences of optical absorption make it possible to determine the type of material conductivity as well as to evaluate the effect of impurities, defects, mechanical stresses in metal layers up to several tens of nanometers thick [2]. In particular, magneto-modulated ellipsometry, or simply magneto-optical ellipsometry (magneto-ellipsometry, in short), allows one to obtain information about changes in the optical properties of a medium in a modulating magnetic field, i.e., to measure magneto-optical (MO) properties. From MO measurements, it is possible to obtain the spectral dependences of the off-diagonal components of the dielectric tensor, to determine the energies of interband transitions of the material and, in combination with the methods of DFT calculation, to analyze the electronic structure of the material [3, 4].

From ellipsometry and magneto-ellipsometry (ME) measurements data, it is possible to get all elements of the dielectric permittivity tensor [5–10] of ferromagnetic layers. In case of an isotropic medium with magnetization being along the  $z$  axis, the tensor takes the following form:

$$[\varepsilon] = \begin{bmatrix} \varepsilon'_{11} - i\varepsilon''_{11} & -i(\varepsilon'_{11} - i\varepsilon''_{11})(Q_1 - iQ_2) & 0 \\ i(\varepsilon'_{11} - i\varepsilon''_{11})(Q_1 - iQ_2) & \varepsilon'_{11} - i\varepsilon''_{11} & 0 \\ 0 & 0 & \varepsilon'_{11} - i\varepsilon''_{11} \end{bmatrix}, \quad (1)$$

where diagonal components of the dielectric constant tensor  $\varepsilon_{11}$  are obtained from the refractive index  $n$  and extinction coefficient  $k$ :

$$\varepsilon_{11} = \varepsilon'_{11} - i\varepsilon''_{11} = (n - ik)^2. \quad (2)$$

One of the characteristics of a magnetized ferromagnetic metal is the MO Voigt complex parameter  $Q = Q_1 - iQ_2$ . Parameter  $Q$  is considered to be proportional to the magnetization in accordance with [5–7] and is included in the dielectric permittivity tensor as a multiplier of the off-diagonal components  $\varepsilon_{xy} = -iQ_{xx}$  [5–7]. The MO parameter makes it possible to describe various MO effects, such as magnetic circular dichroism (MCD) [11], MO Kerr effects [12–15], Faraday effect [16, 17], Voigt effect [17].

However, a significant obstacle to the widespread use of MO methods of *in situ* analysis is the complexity of solving the inverse problem of magneto-ellipsometry, i.e., information on physical properties of the sample should be found from experimental data  $\psi$  and  $\Delta$ . Many scientists work on developing algorithms of ME data analysis in order to find the total dielectric tensor of ferromagnetic layers comparable in thickness to the skin depth. The problem to be solved is how to get information on both optical and magneto-optical properties of the sample from *in situ* measurements, i.e., in the same UHV chamber where the sample is grown and without any additional equipment.

It is known that ellipsometry and magneto-ellipsometry are physical model-dependent. That is why any data processing algorithm is based on the optical model of the sample. The earliest works of Višňovský [18, 19] are the most systematized, since they allow one to analyze a wide variety of systems, from anisotropic crystals to multilayer systems, within the framework of one approach. However, the complexity of the mathematical apparatus of  $4 \times 4$  matrices, based on the Yeh's formalism [20], and the necessity to rotate the sample (conduct the measurements in different geometries) prevents wide use of this approach for *in situ* studies. Researchers often need a simpler, but at the same time reliable way of analyzing experimental data of magneto-ellipsometry. That is why the attempts to develop and apply other algorithms for ME data analysis are still being undertaken by scientists from different countries.

Some authors developed the data processing algorithms for the simplest model [5, 6, 21, 22], which is the model of a homogeneous semi-infinite ferromagnetic medium. They used it to study polycrystalline

permalloy and iron films of thicknesses 150 and 60 nm, respectively. However, this approach is not universal, since it is not enough to use the model of a semi-infinite layer developed for bulk materials and thick films when one needs to interpret the experimental data for ferromagnetic layers of thicknesses comparable to the skin depth in the investigated spectral range. The authors of works [23–25] tried to go beyond the bulk model and developed an approach based on the idea of analyzing changes in ellipsometric parameters  $\delta\psi$  and  $\delta\Delta$  as small corrections to  $\psi_0$ ,  $\Delta_0$  in the transverse Kerr effect. Unfortunately, they limited themselves to considering two models: a bulk ferromagnetic sample and a thin-film sample on a non-magnetic substrate.

The works of the Mok group [26, 27] are an example of difficulties when using  $4 \times 4$  matrices. It was not enough to conduct ellipsometric measurements to characterize the MO properties of the sample. In addition to magneto-optical ellipsometry, they had to use a SQUID to measure the magnetization  $M$  of the sample *ex situ*. It gave them the possibility to work with both thin-film and multilayer systems, but at the same time they have lost the ability to carry out a full cycle of measurements *in situ*. As a result, they obtained information on the diagonal and off-diagonal components of the permittivity tensor but differently from (1), i.e., in order to use the values of measured magnetization they had to redefine the magneto-optical parameter  $Q$  [26] as independent of magnetization by assuming the off-diagonal terms to be  $\varepsilon_{ij}^{\text{MO}} = -iQ_k M_k$ , with  $i, j = 1, 2, 3$ ,  $k = x, y, z$ , respectively.

There is also a number of works [28–33] where the original spectral magneto-ellipsometry complex setup was designed. It allows one to carry out *in situ* measurements of MO parameters and optical parameters at a fixed angle of incidence of light on a ferromagnetic sample and to carry out a joint analysis of reflective spectral ellipsometry measurements and changes in the ellipsometric parameters of a ferromagnetic sample during its magnetization reversal, arising due to the contribution of the MO transverse Kerr effect to the polarization state. It is important to note that there is no need to change the position of a sample and to use additional measuring equipment. The authors introduce data processing algorithms that do not require a large number of measurements aimed at determining all elements of the fourth-order matrices. Instead of  $4 \times 4$  matrices, the analysis of ME data is based on the use of ellipsometric relations, where the magneto-

optical contribution is taken into account as a perturbation. A number of works devoted to such algorithms for bulk media, thin films, and multilayers have already been published [29–33].

As a result, the full dielectric permittivity tensor of a multilayer ferromagnetic medium is obtained according to Eq. (1), where  $Q$  is magnetization-dependent. The developed approach to data processing can be used for in situ analysis of the electronic structure of various thin-film magnetic structures, such as planar MAX systems [11, 34], ensembles of single-domain super-paramagnetic nanoparticles [35], spin glasses [36], etc.

Although the methodological foundations of the generalized magneto-optical ellipsometry are still under development, it is evident that this method is powerful as it gives the values of all components of the dielectric tensor, which include the value of MO parameter  $Q$  [6, 7] also called MO-coupling parameter. From a microscopic view, MO coupling is due to spin-orbit interaction and  $Q$  is due to the first-order spin-orbit coupling [37–39].  $Q$  is of importance for light management in modern integrated-optics devices [16]. One can calculate all MO effects [11–17, 40, 41] using the formulae of phenomenological theory [17, 41, 42] as soon as the value of magneto-optical parameter  $Q$  is found by conducting any MO effects measurements for particular wavelength of the beam light.

In this work, we show the process of finding  $Q$  of Fe of different thickness from ME data using different magneto-optical models and study the behavior of the MO parameter spectra of iron in layered samples with different thickness of Fe layer in order to check if/how  $Q$  is sample- and thickness-dependent.

## 2. SAMPLES DESCRIPTION

Four samples with the structure “ferromagnetic layer | dielectric layer | non-ferromagnetic substrate” were created. The thickest sample (no. 1 in Table 1) was deposited separately from the series of three thin samples (nos. 2–4 in Table 1) to be a test structure. Polycrystalline iron (purity 99.99+%) of various thickness was chosen as the ferromagnetic layer. For the non-ferromagnetic substrate, we used single-crystal silicon wafers with a crystallographic orientation of the surface (100) (purity 99.999+%). The dielectric layer was an artificially prepared amorphous  $\text{SiO}_2$  layer. It is important to note that native oxide which is formed when silicon substrates are stored in air in plastic packaging, was removed by etching. Native oxides can lead to a difference in its physicochemical properties from sample to sample with an unpredictable effect on the Fe layer. Therefore, to improve the reproducibility of the properties of the  $\text{SiO}_2$ –Fe boundary and the chemical composition of the oxide, the technology of artificial formation of  $\text{SiO}_2$  was

**Table 1.**  $\text{SiO}_2$  and Fe thicknesses from XRF data

Sample no.	$d(\text{SiO}_2)$ , nm, according to in situ spectral ellipsometry data	$d(\text{Fe})$ , nm, according to the XRF data
1	$3.8 \pm 0.2$	$160.5 \pm 0.8$
2	$0.7 \pm 0.2$	$77.0 \pm 0.6$
3	$1.8 \pm 0.2$	$33.5 \pm 0.6$
4	$1 \pm 0.2$	$11.5 \pm 0.6$

used. The treatment of the substrate and the creation of the  $\text{SiO}_2$  layer were carried out according to the method from [43] with thickness control by *in situ* spectral ellipsometry and a simple single-layer ellipsometric model use. Optical constants were taken from [28] for Si and from [44] for  $\text{SiO}_2$ . The  $\text{SiO}_2$  thickness was measured after the samples were annealed in UHV up to 670 K by direct passage of current through the substrate. The deposition of polycrystalline iron on a  $\text{Si}(100)|\text{SiO}_2$  substrate at room temperature was carried out in an UHV (residual atmosphere  $10^{-7}$  Pa) by thermal evaporation from an auto-crucible source with electron-beam heating. The sample was placed on a special holder [28]. The iron deposition rate was monitored by single-wavelength ellipsometry at a wavelength of 577 nm using a simultaneous calculation of the thickness and optical constants of the growing layer according to the method from [45]. For all samples, the calculated Fe deposition rate during the ellipsometric control was 1.3 nm/min.

In situ magneto-ellipsometric measurements in the geometry of the transverse MO Kerr effect were carried out directly in the UHV technological chamber, after the synthesis of the structures. Measurements were carried out sequentially in the entire spectral range from 1.25 to 3.5 eV after forward and reverse magnetization of the sample with subtraction of the average values for the demagnetized state [46]. A high-speed spectral ellipsometer Ellips-1891 [47] with an additional device for setting the magnetic field on the sample was used for these measurements. The ferromagnetic saturation field of the sample was set at  $\pm 200$  mT according to the results of preliminary measurements of the magnetization reversal loop.

Subsequently, after a full cycle of in situ ellipsometric and magneto-ellipsometric measurements (Fig. 1), all synthesized samples were removed from the UHV and studied by X-ray spectral fluorescence analysis to define more precisely the thickness of the deposited iron in terms of a density of  $7874 \text{ kg/m}^3$  (Table 1).

For the thinnest sample, additional studies were carried out by means of X-ray photoelectron spectroscopy (see Appendix).

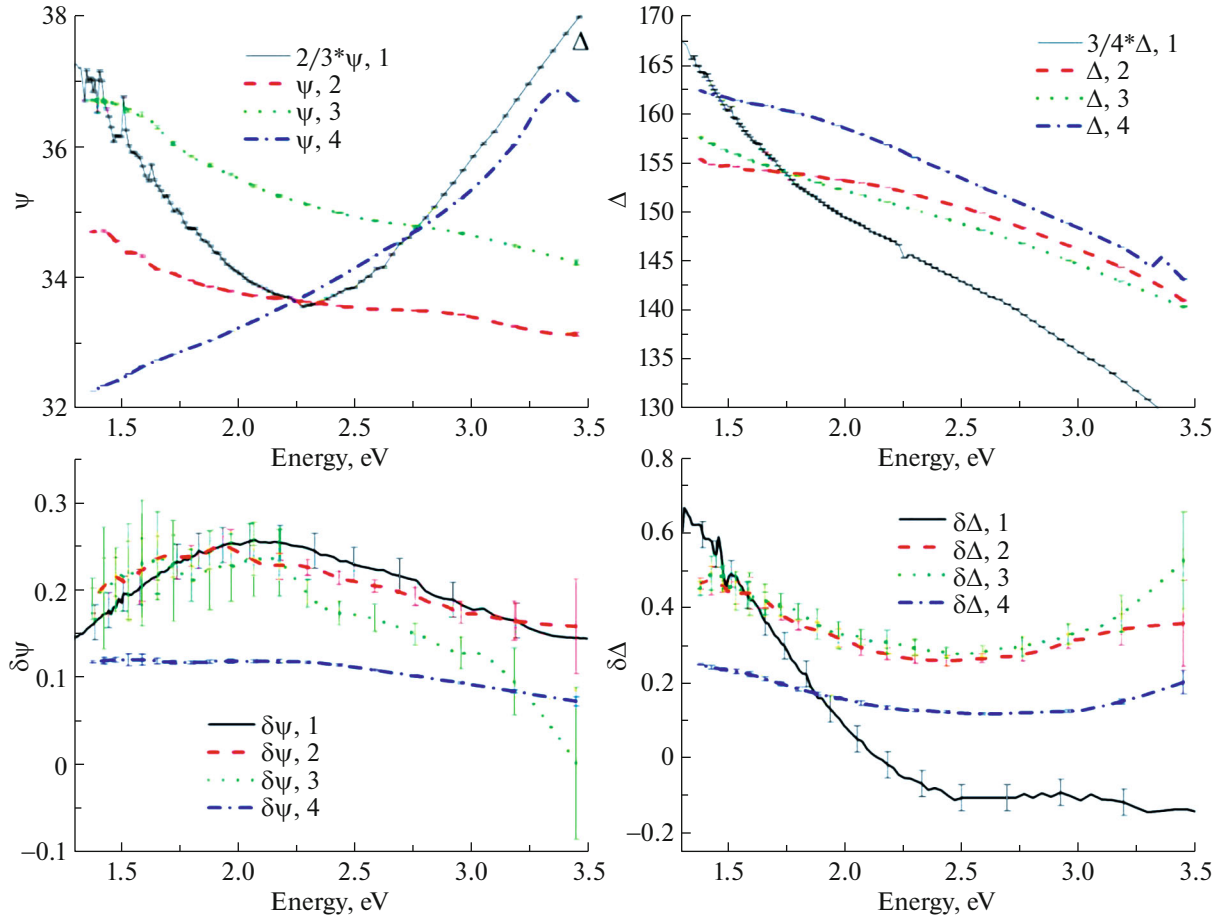


**Fig. 1.** Experimental ellipsometry ( $\psi$ ,  $\Delta$ ) and magneto-ellipsometry ( $\delta\psi$ ,  $\delta\Delta$ ) data. 1–4 in the legends refer to the sample numbers in Table 1, the values of  $\psi$ ,  $\Delta$  for sample 1 are normalized so that they could be compared to others. Error-bars are calculated as rms and provided for all samples in this figure, however their size for some curves is comparable with the thickness of the curve.

### 3. MAGNETO-ELLIPSOMETRY DATA PROCESSING

#### 3.1. Method of Finding the Magneto-Optical Parameter $Q$ from Experimental Magneto-Ellipsometric Data for Various Models of Reflecting Ferromagnetic Nanostructures

In this work, the MO parameter  $Q = Q_1 - iQ_2$  is considered to be proportional to the magnetization in accordance with [5–7]. We used this approach because the setup [28] used in this study was specifically designed for in situ investigations, which means that all ellipsometry and ME measurements are held in the same vacuum chamber and no additional equipment is needed to find all components of dielectric permittivity tensor.

The key ideas of the approach used to interpret magnetic field modulated spectral ellipsometric measurements of a ferromagnetic nanostructure using the transverse MO Kerr effect are published in [29] and [30]. Within the framework of this approach, one can

analyze magneto-optical ellipsometry data using the following models:

- a model of a homogeneous semi-infinite ferromagnetic medium [30];
- a model “thin ferromagnetic film | non-magnetic substrate” [31];
- a two-layer model “ferromagnetic layer | non-magnetic buffer layer | non-magnetic substrate” [32];
- a multilayer model [33].

A short description of the required actions to get the values of MO parameter  $Q$  is provided in Table 2.

The error of the MO parameter  $Q$  is calculated by the formula

$$\Delta Q = \sqrt{\sum_j \left( \Delta x_j \frac{\partial Q}{\partial x_j} \right)^2}, \quad (3)$$

where  $Q = Q(x_j)$ ,  $x_j$  are directly measurable independent quantities  $\varphi_0$ ,  $\psi_0$ ,  $\Delta_0$ ,  $\delta\psi$ ,  $\delta\Delta$ ,  $d$  with root-mean-square deviation  $\Delta x_j$ .

**Table 2.** Getting MO parameter  $Q$  using a proper model of a sample

No.	Step	Obtained parameters
1	Conducting ellipsometry and magneto-optical ellipsometry measurements	Experimental: $\Psi_0, \Delta_0, \delta\Psi, \delta\Delta$
2	Calculating optical properties	$n, k$
3	Calculating ellipsometric parameters from reflection coefficients [29–33]	Theoretical: $\Psi_0, \Delta_0, \delta\Psi, \delta\Delta$
4	Calculating magneto-optical parameter by minimizing the sum of squares of the difference between the magneto-ellipsometric parameters calculated in Step 3 and measured during the experiment (Step 1) by the Nelder–Mead algorithm [48] for each wavelength	$Q$
5	Estimating the error of the MO parameter $Q$ [49]	$\Delta Q$

Thus, based on the results of processing the experimental data, it is possible to obtain information on the MO properties of the material, and it is also possible to calculate the values of all components of the dielectric permittivity tensor of a magnetized ferromagnetic metal.

### 3.2. Analysis of a Sample with a Bulk Fe Layer

This section presents experimental verification of the applicability of the MO models used in the algorithms published in [30–33], the algorithms are tested on the thick nanostructure Fe|SiO<sub>2</sub>|Si.

The Fe|SiO<sub>2</sub>|Si sample with an iron thickness of  $160.5 \pm 0.8$  nm (no. 1 in Table 1) was used as a test structure to check the work of the developed algorithms using various models of reflecting systems. This sample growth was reported in details in [30]. The thickness of the iron layer in sample 1 is many times greater than the skin depth in the investigated spectral range. That is why the simplest model of a semi-infinite ferromagnetic medium should be sufficient for

it. Any complication of the model should not lead to a change in the calculation results. For simplicity of the calculation, we did not take into account a thin rough layer on the sample surface, the thickness of which usually does not exceed 0.6 nm [46].

The results of calculating the MO parameter  $Q$  for sample 1 using various models are presented in Fig. 2, where  $a, b, c$  are the models mentioned in Subsection 3.1.

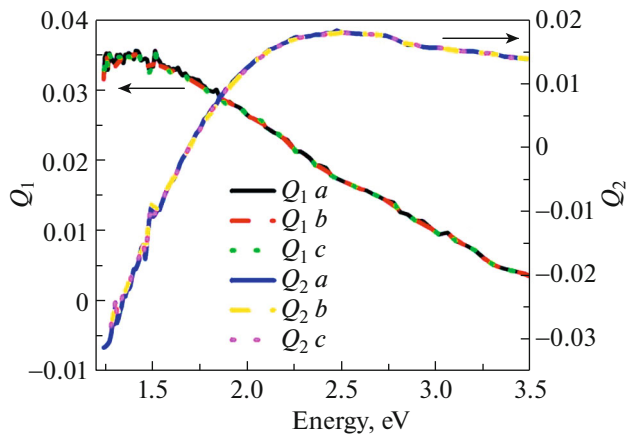
In [30], where only model  $a$  was used for calculations, it was shown that the values of  $Q$  of this sample, are in good agreement with literature data [5]. Therefore, it is possible to use the developed algorithms for calculating  $Q$  of ferromagnetic Fe films of various thicknesses.

### 3.3. Analysis of Samples with Different Thicknesses of the Polycrystalline Fe Layer

In this section, magneto-optical models [30, 32, 33] are used to calculate MO parameter  $Q$  and are directly compared in terms of the dissimilarities between obtained spectral curves; MO properties of iron in layered samples with different Fe thickness are discussed.

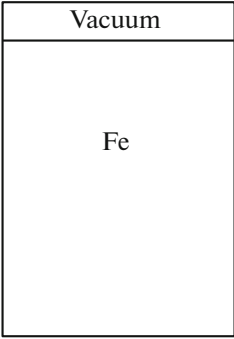
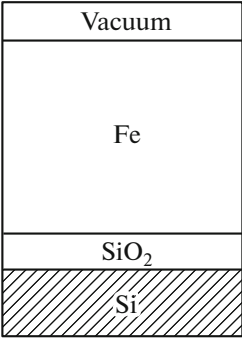
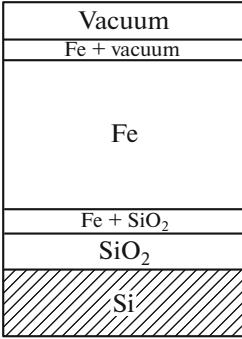
The calculations of the values of the MO parameter  $Q$  for a series of three Fe|SiO<sub>2</sub>|Si samples with different thicknesses of the iron and silicon dioxide layers (nos. 2–4 in Table 1) were done. The  $Q$  spectra were calculated using three models (Table 3): models  $a$  and  $c$ , mentioned in Subsection 3.1, and model  $d$  being a multilayer medium that contains mixed interface layers and a ferromagnetic layer [33]. Model  $b$  was not used here as its application would be artificial.

In model  $d$ , the thicknesses of Fe–vacuum and SiO<sub>2</sub>–Fe interfaces were 0.58 and 0.12 nm, respectively. The thicknesses of these interfaces correspond to the rms roughness for similar structures from [43]. The volume fraction of iron in both interfaces was chosen to be 50% for simplicity in using Bruggeman model [50] and in accordance with the work [43], where the rms roughness for similar structures was obtained. The rms calculations [43] implied the prob-



**Fig. 2.** Values of the real and imaginary parts of the MO parameter  $Q = Q_1 - iQ_2$ , calculated using various models of the reflecting system for sample 1.

**Table 3.** Computational models

Model	<i>a</i>	<i>c</i>	<i>d</i>
	A model of a homogeneous semi-infinite ferromagnetic medium	A two-layer model “ferromagnetic layer   non-magnetic buffer layer   non-magnetic substrate”	A multilayer medium
Our samples 2, 3, 4			

ability to find an atom of Fe or SiO<sub>2</sub> (or vacuum if it is an upper interface) at a specific point on the plane lying in the middle of the mixed layer to be close to 50%, since the structure is not ordered (the iron layer is polycrystalline, the SiO<sub>2</sub> sub-layer has an amorphous irregular structure, which is supported by microscopy studies [43]). Adjusting of the percentage of Fe may lead to the changes in  $n$ ,  $k$  spectral curves which in turn changes the values of the complex magneto-optical parameter  $Q$ ; however, for the reported samples these changes are small relative to the error. We estimated these changes within  $\pm 5\%$  and they turned out to be 4–5 orders of magnitude less than the error in setting the thickness of the main iron layer. Apparently, this depends on the ratio of the thickness of the mixed layer to the thickness of the main layer

and the surface relief of the film. The possible MO contribution from both interface layers was not taken into account in this work because the value of the magnetization of iron in both layers is relatively small in comparison to the main iron layer: less than 3.5% based on the number of Fe atoms for sample 4 with the thinnest ferromagnetic layer (without taking into account the weakening of the magnetic moment due to porosity and defects in the crystal structure). To calculate the spectra of the permittivity of the mixed layers, the Bruggeman’s effective medium model [1, 51] was used.

All layers and media in the calculations were considered to be isotropic, homogeneous, with sharp boundaries. When analyzing the experimental ME data, it was necessary to calculate the optical parameters  $n$ ,  $k$  of the iron layer and all mixed layers (Figs. 3–5); for this, the Spectroscan program (Version 1.10) was used.

The spectral dependence of the dielectric permittivity  $\epsilon_{11}$  for SiO<sub>2</sub> was used from [44]. The dielectric permittivity  $\epsilon_{11}$  of silicon was measured by the method of spectral ellipsometry from a single-crystal Si (100) substrate at room temperature [46].

The law of error propagation [49] was used to numerically calculate the errors of the refractive index  $n$  and extinction coefficient  $k$  of the investigated ferromagnetic layer. The following experimental errors were used: the accuracy of setting the angle of incidence of the optical beam according to the in situ adjustment of the optical measurement scheme before the deposition of iron was  $\pm 0.02^\circ$ ; the accuracy of in situ ellipsometry measurements of the SiO<sub>2</sub> layer thickness before iron deposition was  $\pm 0.02$  nm; the accuracy of measuring the upper interface layer thickness from the AFM data was  $\pm 0.1$  nm [52]; the error in estimating the thickness of the lower interface layer was  $\pm 0.06$  nm; the typical accuracy of determining the

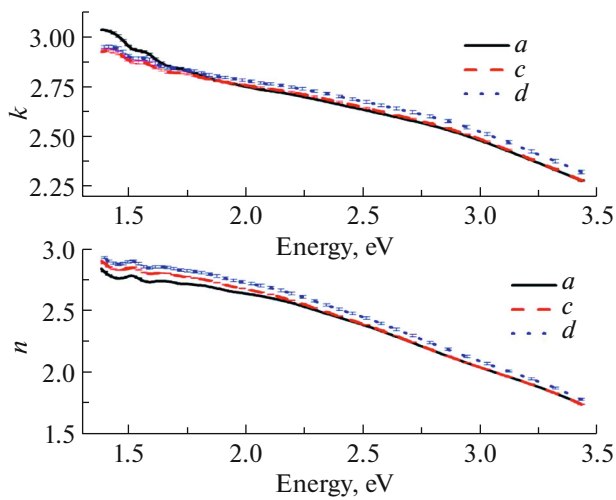


**Fig. 3.** Refractive index  $n$  and extinction coefficient  $k$  of Fe layer in sample 2 according to models  $a$ ,  $c$  and  $d$ . Thickness of Fe layer is 77.0 nm.

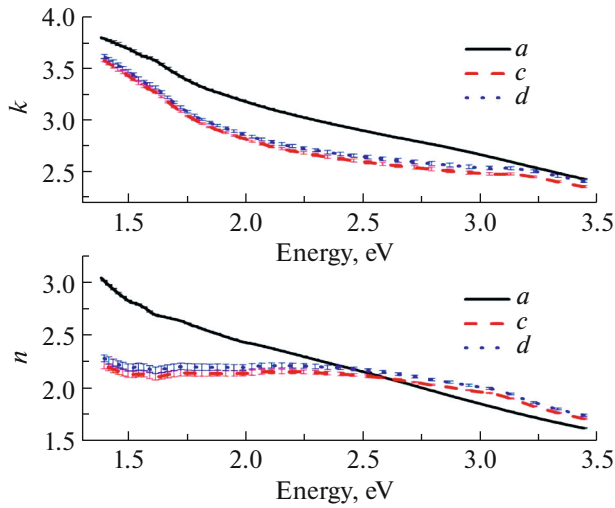


**Fig. 4.** Refractive index  $n$  and extinction coefficient  $k$  of Fe layer in sample 3 according to models  $a$ ,  $c$  and  $d$ . Thickness of Fe layer is 33.5 nm.

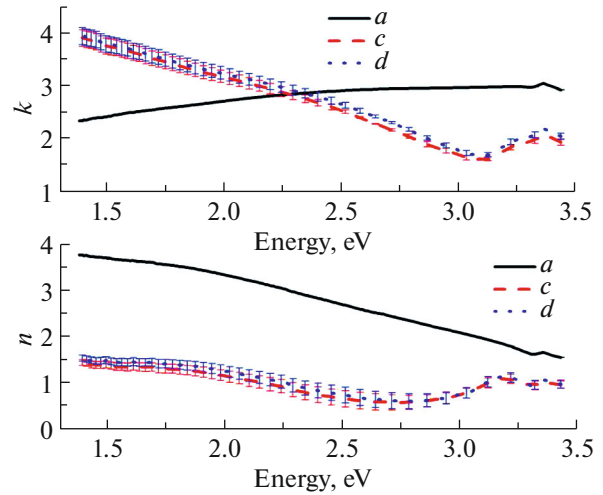


**Fig. 5.** Refractive index  $n$  and extinction coefficient  $k$  of Fe layer in sample 4 according to models  $a$ ,  $c$  and  $d$ . Thickness of Fe layer is 11.5 nm.

thickness of thin Fe layer by X-ray spectral fluorescence analysis was  $\pm 0.6$  nm; the difference in the volume fraction of Fe in the upper and lower interface layers taking into account the different geometry of the interface boundary was  $\pm 10\%$  [53]. For the tabulated values of the optical properties of Si and SiO<sub>2</sub>, the errors of the refractive index and extinction coefficient were set as  $\pm 0.001$  based on the order of the least decimal place. It should be noted that errors in optical properties of the substrate and SiO<sub>2</sub> layer influence several orders of magnitude less on the error of  $n$ ,  $k$  of ferromagnetic layer than errors in determining this ferromagnetic layer thickness.

Optical properties of the Fe layers in Figs. 3–5 that were determined from ellipsometry for samples 2–4 show how they vary with iron thicknesses, which is important to be taken in account while determining MO parameter  $Q$ . Figures 3–5 also allow to estimate the impact of the roughness of the layers in samples 2–4 which could be expected to be significant, as ellipsometry is a high-sensitive technique, especially for absorbing materials. One can see that the refractive index  $n$  and extinction coefficient  $k$  calculated by models  $c$  and  $d$  do not match within the margin of error in all investigated spectral range. That is why it can be concluded that an inclusion of interface layers into the data processing algorithms for accounting the roughness affect the optical properties that are extracted.

Let us consider in which cases the simplest model  $a$  is sufficient to investigate MO properties, and when it is required to apply the most complex model  $d$ , which takes into account the Fe-containing nonmagnetic porous interface layer, ferromagnetic Fe layer, nonmagnetic mixed Fe–SiO<sub>2</sub> interface layer, non-

magnetic SiO<sub>2</sub> layer, and non-magnetic Si substrate (Table 3). For this, the MO parameter  $Q$  was calculated from spectral ME measurements for iron layer in samples 2, 3, and 4 (Figs. 6–8).

The values of the refractive index  $n$  and extinction coefficient  $k$  that were used while calculating the MO parameter were taken from Figs. 3–5 depending on the corresponding model  $a$ ,  $c$ , or  $d$ .

Figures 6–8 show that the thickness of the ferromagnetic layer has a significant impact on the calculation results for all models. One can see that there is correlation of the discrepancy between the  $Q$  curves for different models in different parts of the spectrum

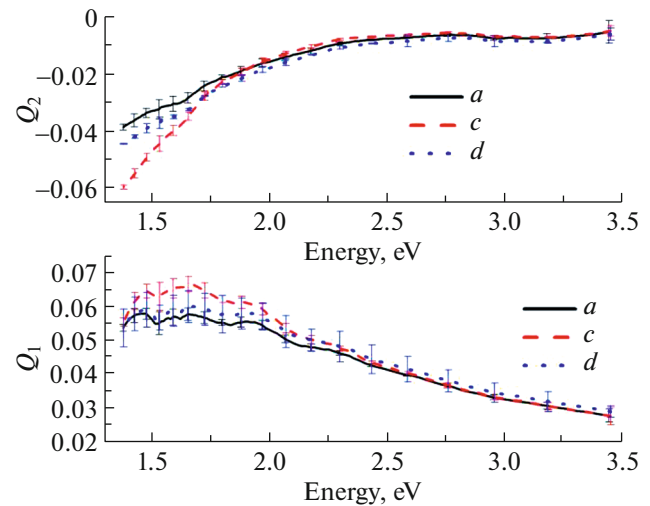


**Fig. 6.** The MO Voigt parameter  $Q$  according to models  $a$ ,  $c$ , and  $d$  for Sample 2 with a Fe layer thickness of 77.0 nm.

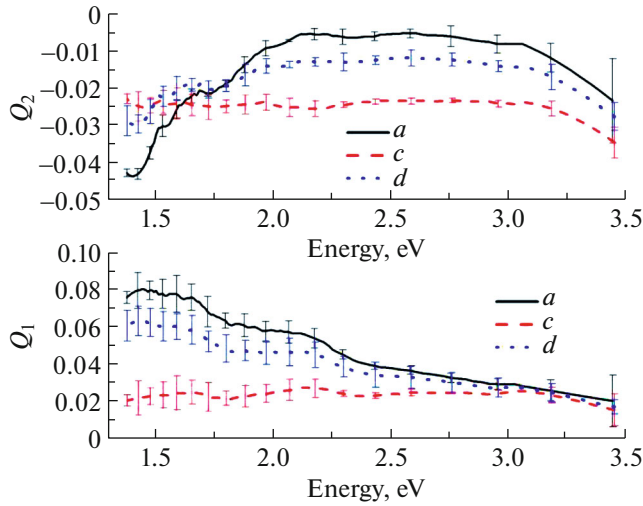


**Fig. 7.** The MO Voigt parameter  $Q$  according to models  $a$ ,  $c$ , and  $d$  for sample 3 with a Fe layer thickness of 33.5 nm.

for samples 2 and 3 and the spectral dependence of the skin depth [1] of iron (Fig. 9) given by the formula

$$d_p = \lambda / (4\pi k), \quad (4)$$

where  $\lambda$  is the radiation wavelength,  $k$  is the extinction coefficient. As the iron thickness decreases from sample 2 to sample 3, there is also a decrease of the probe wavelength, at which the discrepancies in  $Q_1$  and  $Q_2$  spectra between the models begin to exceed the value of the experimental measurement error.

It is important to note that for the imaginary part of the magneto-optical parameter  $Q_2$ , the spectral dependences obtained using the model of a homogeneous semi-infinite medium diverge from other spectral dependences for all samples, and for thin

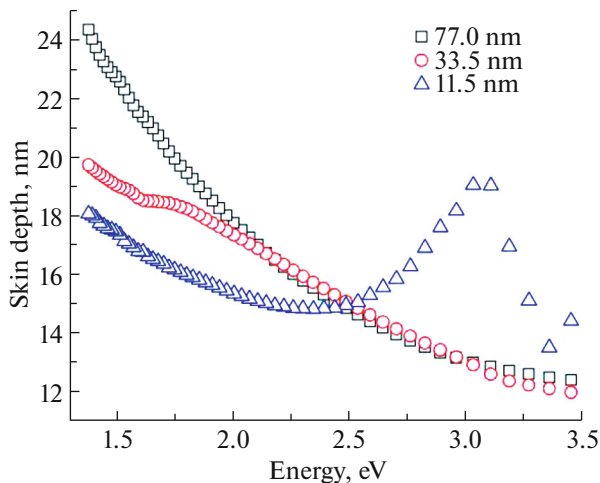


**Fig. 9.** Spectral dependence of the Fe skin depth according to spectral ellipsometry data for samples 2–4.

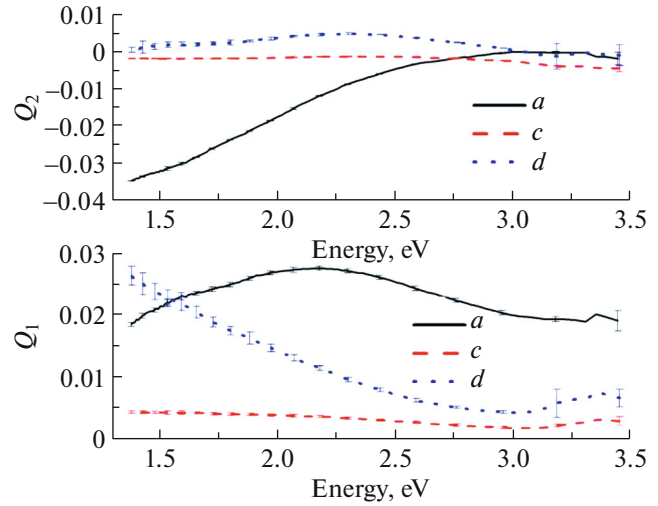


**Fig. 8.** The MO Voigt parameter  $Q$  according to models  $a$ ,  $c$ , and  $d$  for sample 4 with a Fe layer thickness of 11.5 nm.

samples the discrepancy is observed over a wider energy range. The spectral dependence of  $Q_2$ , obtained using model  $a$ , diverges from the results of the other models for sample 2 in the range less than 1.75 eV.

Accordingly, when calculating the complex magneto-optical parameter  $Q$  for the sample with a ferromagnetic layer thickness of 77 nm, it is sufficient to restrict ourselves to a model of a semi-infinite medium for incident radiation energies above 1.75 eV; for lower energies, it is necessary to take into account the presence of a substrate (see Fig. 6). At the same time, based on Fig. 7, it can be concluded that for the sample with a ferromagnetic layer thickness of 33.5 nm, the semi-infinite medium model does not work. It follows from Fig. 8 that for sample 4, the two-layer model  $c$  is more accurate than model  $a$ .

As for the discrepancy in calculations between models  $c$  and  $d$ , for the thickest sample 2, as expected, the multilayer model  $d$ , taking into account intermix layers, is redundant. For samples 3 and 4 the multilayer model  $d$ , where Fe and  $\text{SiO}_2$  layers are separated by a mixed layer and an additional non-magnetic mixed layer at the Fe–vacuum interface is taken into account, is more preferable than model  $c$  in the entire spectral range. This can be explained due to the physical meaning of MO coupling parameter  $Q$ , related to spin–orbit coupling. As far as “spin–orbit coupling is known to be altered at the interfaces” [37] and playing significant role in ferromagnetic–non-ferromagnetic interface contributions to magneto-optical Kerr effect [54], inclusion of interfaces Fe–vacuum and Fe– $\text{SiO}_2$  in the samples  $\text{Fe}|\text{SiO}_2|\text{Si}$  results in the change of MO parameter  $Q$ . The thinner the sample is, the stronger the change is.



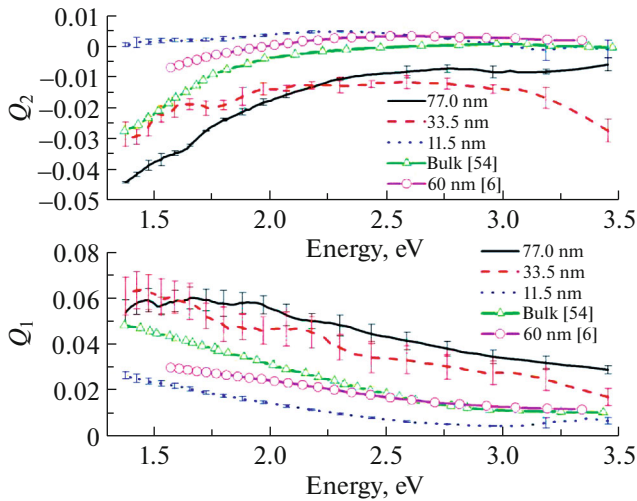


**Fig. 10.** Dispersions of the real and imaginary components of the magneto-optical parameter  $Q$  of the Fe layer of samples 2, 3, 4 in comparison with the literature data.

Thus, taking into account the correlation of the skin depth and the superposition of the results of calculating  $Q$  for the ferromagnetic layer of different thickness by different models use, it can be concluded that the surface sensitivity of the *in situ* magneto-ellipsometry technique is equal to  $\sim 3.9$  skin depths (19.5 nm per 1.75 eV) for the model of a semi-infinite medium, which agrees with the estimates of the sensitivity of the ellipsometry method in  $\sim 5$  skin depths from [1]. This value of  $5d_p$  is well-known for experts in classical ellipsometry measurements being held without applying external magnetic field, and in this work we demonstrate that it is sensible to take it into account when analyzing magneto-optical response as well by checking whether the sample thickness is more than  $4-5d_p$  for using a model of a homogeneous semi-infinite ferromagnetic medium in magneto-optical ellipsometry. If this condition is not satisfied then other layers should be taken into account when searching for MO properties of the sample.

In Fig. 10, MO parameter  $Q$  calculated using the most complex d model for samples 2, 3, 4 is compared with literature data for bulk Fe samples [55] and Fe films 60-nm thick in [6].

There is a qualitative agreement. However, a quantitative comparison shows a discrepancy in the spectra not only between our samples, but also the data of other authors, which, on the one hand, indicates, the extremely high sensitivity of the method to the electronic structure and state of the surface of the ferromagnetic film, on the other hand, it demonstrates that iron Voigt parameter  $Q$ , defined according to (1), is very sample-dependent and thickness-dependent. The fact that thin layers have different optical properties than bulk layers definitely contributed to the deviation between the determined MO parameters  $Q$ . It is

in agreement with [37, 54], where it is reported that  $Q$  values are very dissimilar between samples, because of the interface contributions, different angles of incidence and incident light polarization during MO measurements, various optical properties, and thicknesses of the interface layers. Though earlier some authors expected off-diagonal elements of dielectric tensor to be thickness independent [56], nowadays there is already a number of published works which report on the thickness dependence of  $\epsilon_{xy}$  [12, 37, 54, 56–58]. The results of the present work also support the latter idea.

## CONCLUSIONS

For Fe|SiO<sub>2</sub>|Si samples with Fe layer thicknesses of 160.5, 77.0, 33.5, and 11.5 nm, obtained under UHV conditions, *in situ* measurements of ellipsometry and magneto-ellipsometry spectra were carried out in the range 1.38–3.45 eV, in fields of ferromagnetic saturation  $\pm 200$  mT at room temperature. From the measured data, spectra of the complex magneto-optical Voigt parameter  $Q$  were calculated using the model of a homogeneous semi-infinite medium, a two-layer model and a multilayer model with one ferromagnetic layer. The calculation algorithms consisted of taking into account magneto-ellipsometry measurements as small perturbations to ellipsometry measurements on a demagnetized sample. The obtained Voigt parameter allows one to find the off-diagonal components of the dielectric permittivity tensor of a ferromagnetic material, analyze its electronic structure and calculate any magneto-optical effects.

According to our findings, when the thickness of the absorbing ferromagnetic layer is more than 4 times the skin depth in the spectral range of interest, it is irrational to use complex multiparameter models of the reflecting surface. If the outer rough layer is not taken into account, it is enough to use a simple model of a semi-infinite medium, the versions of which have been developed by many authors, including our team. Also, for such thick samples the value of magneto-optical Voigt parameter can be taken from the reference books while for thinner samples the value of  $Q$  is sample-dependent and thickness-dependent.

However, tabulated parameters strongly vary because many factors contribute to the optical and magneto-optical parameters of the ferromagnetic film, e.g., thickness, quality, angles of incidence and, remarkably, interface contributions that are related to spin-orbit coupling. That is why for thin ferromagnetic films it is preferable to use a multilayer model, which takes into account intermix layers, in the magneto-ellipsometry data processing algorithms.

## APPENDIX

For sample 4, additional studies were carried out using X-ray photoelectron spectroscopy (XPS) with

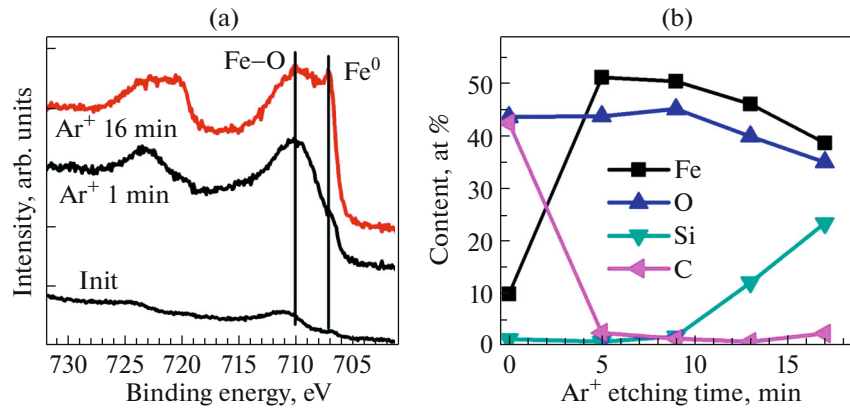


Fig. 11. (a) X-ray photoelectron spectra and (b) atomic content in the surface layer of sample 4.

layer-by-layer etching of the sample with argon ions (Fig. 11) to obtain information on the structure and elemental composition of the sample.

X-ray photoelectron spectra were recorded using a SPECS photoelectron spectrometer with a PHOIBOS 150 MCD 9 hemispherical energy analyzer under excitation by  $MgK_{\alpha}$  (1253.6 eV) radiation from the magnesium anode of the X-ray tube and the normal angle of photoelectron registration. The transmission energies of the energy analyzer were 20 eV for survey spectra and 8 eV for high-resolution spectra. To obtain a depth profile of elements, a PU-IQE 12/38 (SPECS) argon ion source was used, the argon ion energy was 2.6 keV, and the ion current was 60  $\mu$ A. The spectra were processed with the CasaXPS software package.

The  $Fe2p$  spectra show the presence of metallic iron with a binding energy of  $\sim 706.8$  eV and, probably, several oxide phases that contain  $Fe^{3+}$  and  $Fe^{2+}$  after removal of the strongly oxidized surface layer by ion etching. The total proportion of elemental iron in the spectra increases with etching time from  $\sim 20$  to  $\sim 50\%$ . The occurrence of significant quantities of carbon and oxygen on the film surface is caused by exposure of the sample to the atmosphere during transfer to the XPS spectrometer. Taking into account the ex situ oxidation, the atomic concentration of iron is consistent with the data on thickness measurements by XRF.

#### FUNDING

The research was supported by the government of the Russian Federation (agreement no. 075-15-2019-1886).

#### ACKNOWLEDGMENTS

We thank the Krasnoyarsk Regional Center of Research Equipment of Federal Research Center “Krasnoyarsk Science Center SB RAS” for the opportunity to record X-ray photoelectron spectra using a SPECS photoelectron spectrometer (<http://ccu.kirensky.ru/info/19/>).

#### CONFLICT OF INTEREST

The authors declare that they have no conflicts of interest.

#### REFERENCES

1. H. Fujiwara, *Spectroscopic Ellipsometry: Principles and Applications* (Wiley, New York, 2007).
2. C. Ma, H. G. Wang, P. J. Zhao, J. Bao Xu, A. M. Chang, L. Wang, and L. Bian, *Mater. Lett.* **136**, 225 (2014).
3. J. Mack, M. J. Stillman, and N. Kobayashi, *Coord. Chem. Rev.* **251**, 429 (2007).
4. M. L. Kirk and K. Peariso, *Curr. Opin. Chem. Biol.* **7**, 220 (2003).
5. R. Rauer, G. Neuber, J. Kunze, J. Bäckström, and M. Rübhausen, *Rev. Sci. Instrum.* **76**, 023910 (2005).
6. G. Neuber, R. Rauer, J. Kunze, T. Korn, C. Pels, G. Meier, U. Merkt, J. Bäckström, and M. Rübhausen, *Appl. Phys. Lett.* **83**, 4509 (2003).
7. A. V. Sokolov, *Optical Properties of Metals* (GIFML, Moscow, 1961) [in Russian].
8. T. Haider, *J. Electromagn. Appl.* **7**, 17 (2017).
9. A. Molina-Sánchez, G. Catarina, D. Sangalli, and J. Fernandez-Rossier, *J. Mater. Chem. C* **8**, 8856 (2020).
10. K. W. Wierman, J. N. Hilfiker, R. F. Sabiryanov, S. S. Jaswal, R. D. Kirby, and J. A. Woollam, *Phys. Rev. B* **55**, 3093 (1997).
11. S. Lyaschenko, O. Maximova, D. Shevtsov, S. Varnakov, I. Tarasov, U. Wiedwald, J. Rosen, S. Ovchinnikov, and M. Farle, *J. Magn. Magn. Mater.* **528**, 167803 (2021).
12. I. D. Lobov, PhD Thesis (Mikheev Inst. Met. Phys., Ural Branch Russ. Acad. Sci., Yekaterinburg, 2018). [http://imp.uran.ru/sites/default/files/disertation/2018\\_09/diss\\_lobov\\_bez\\_podpisi.pdf](http://imp.uran.ru/sites/default/files/disertation/2018_09/diss_lobov_bez_podpisi.pdf).
13. V. M. Mayevsky and G. A. Bolotin, *Fiz. Met. Metallogr.* **32**, 1168 (1971).
14. V. I. Belotelov, PhD Thesis (Moscow State Univ., Moscow, 2012).
15. A. K. Zvezdin and V. A. Kotov, *Magneto-Optics of Thin Films* (Nauka, Moscow, 1988) [in Russian].

16. V. I. Belotelov and A. K. Zvezdin, *J. Opt. Soc. Am. B* **22**, 286 (2005).
17. Linear magneto-optical effects in ferromagnets in reflected light (Moscow State University, Moscow, 2010). [http://nano.msu.ru/files/systems/4\\_2010/practical/38\\_full.pdf](http://nano.msu.ru/files/systems/4_2010/practical/38_full.pdf).
18. Š. Višňovský, *Czechosl. J. Phys. B* **36**, 625 (1986).
19. Š. Višňovský, R. Lopušník, M. Bauer, J. Bok, J. Fassbender, and B. Hillebrands, *Opt. Express* **9**, 121 (2001).
20. P. Yeh, *Surf. Sci.* **96**, 41 (1980).
21. G. Neuber, R. Rauer, J. Kunze, J. Backstrom, and M. Rübhausen, *Thin Solid Films* **455–456**, 39 (2004).
22. A. Berger and M. R. Pufall, *Appl. Phys. Lett.* **71**, 965 (1997).
23. O. Bakradze, *J. Opt. Technol.* **66**, 442 (1999).
24. O. Bakradze, *J. Opt. Technol.* **72**, 225 (2005).
25. O. Bakradze, Z. Alimbarashvili, and R. Janelidze, arXiv: 0909.2977 (2005).
26. K. Mok, G. J. Kovács, J. McCord, L. Li, M. Helm, and H. Schmidt, *Phys. Rev. B* **84**, 094413 (2011).
27. K. Mok, N. Du, and H. Schmidt, *Rev. Sci. Instrum.* **82**, 033112 (2011).
28. D. V. Shevtsov, S. A. Lyashchenko, and S. N. Varnakov, *Instrum. Exp. Tech.* **60**, 759 (2017).
29. O. A. Maximova, N. N. Kosyrev, I. A. Yakovlev, D. V. Shevtsov, S. A. Lyaschenko, S. N. Varnakov, and S. G. Ovchinnikov, *J. Magn. Magn. Mater.* **440**, 153 (2017).
30. O. A. Maximova, N. N. Kosyrev, S. N. Varnakov, S. A. Lyaschenko, I. A. Yakovlev, I. A. Tarasov, D. V. Shevtsov, O. M. Maximova, and S. G. Ovchinnikov, *J. Magn. Magn. Mater.* **440**, 196 (2017).
31. O. A. Maximova, N. N. Kosyrev, S. N. Varnakov, S. A. Lyashchenko, and S. G. Ovchinnikov, *IOP Conf. Ser.: Mater. Sci. Eng.* **155**, 012030 (2017).
32. O. A. Maximova, S. G. Ovchinnikov, N. N. Kosyrev, and S. A. Lyaschenko, *J. Sib. Fed. Univ., Math. Phys.* **10**, 223 (2017).
33. O. A. Maximova, S. A. Lyaschenko, S. N. Varnakov, and S. G. Ovchinnikov, *Def. Dif. Forum* **386**, 131 (2018).
34. M. W. Barsoum, in *Ceramics Science and Technology*, Ed. by R. Riedel and I.-W. Chen, 1st ed. (Wiley-VCH, Weinheim, 2010), p. 299.
35. S. P. Gubin, *Magnetic Nanoparticles* (Wiley, New York, 2009).
36. E. Bolthausen and A. Bovier, *Spin Glasses* (Springer, Berlin, 2007).
37. M. Buchmeier, R. Schreiber, D. E. Bürgler, and C. M. Schneider, *Phys. Rev. B* **79**, 064402 (2009).
38. J. Kunes, *Physica Scripta* **109**, 116 (2004).
39. M.-F. Li, T. Ariizumi, and S. Suzuki, *J. Phys. Soc. Jpn.* **76**, 054702 (2007).
40. S. N. Varnakov, PhD Thesis (Fed. Res. Center Krasnoyarsk Sci. Center, Kirensky Inst. Phys., Sib. Branch Russ. Acad. Sci., Krasnoyarsk, 2017).
41. G. S. Krinchik, *Physics of Magnetic Phenomena* (Moscow State University, Moscow, 1976) [in Russian].
42. G. S. Landsberg, *Optics* (Nauka, Moscow, 1976) [in Russian].
43. N. V. Volkov, A. S. Tarasov, E. V. Eremin, S. N. Varnakov, S. G. Ovchinnikov, and S. M. Zharkov, *J. Appl. Phys.* **109**, 123924 (2011).
44. I. H. Malitson, *J. Opt. Soc. Am.* **55**, 1205 (1965).
45. I. A. Tarasov, N. N. Kosyrev, S. N. Varnakov, S. G. Ovchinnikov, S. M. Zharkov, V. A. Shvets, S. G. Bondarenko, and O. E. Tereshchenko, *Tech. Phys.* **57**, 1225 (2012).
46. O. A. Maximova, S. A. Lyaschenko, M. A. Vysotin, I. A. Tarasov, I. A. Yakovlev, D. V. Shevtsov, A. S. Fedorov, S. N. Varnakov, and S. G. Ovchinnikov, *JETP Lett.* **110**, 166 (2019).
47. N. N. Kosyrev, V. N. Zabluda, I. A. Tarasov, S. A. Lyashchenko, D. V. Shevtsov, S. N. Varnakov, and S. G. Ovchinnikov, RF Patent No. 2560148 (2015).
48. J. A. Nelder and R. Mead, *Comput. J.* **7**, 308 (1965).
49. H. H. Ku, *J. Res. Natl. Bureau Stand.* **70C**, 262 (1966).
50. R. W. Collins, I. An, H. Fujiwara, J. Lee, Y. Lu, J. Koh, and P. I. Rovira, *Thin Solid Films* **313–314**, 18 (1998).
51. L. A. Golovan, V. Yu. Timoshenko, and P. K. Kashkarov, *Phys. Usp.* **50**, 595 (2007).
52. J. Koh, Y. Lu, C. R. Wronski, Y. Kuang, R. W. Collins, T. T. Tsong, and Y. E. Strausser, *Appl. Phys. Lett.* **69**, 1297 (1996).
53. D. E. Aspnes, J. B. Theeten, and F. Hottier, *Phys. Rev. B* **20**, 3292 (1979).
54. J. Hamrle, M. Nyvlt, S. Visnovsky, R. Urban, P. Beauvillain, R. Megy, J. Ferre, L. Polerecky, and D. Renard, *Phys. Rev. B* **64**, 155405 (2001).
55. G. S. Krinchik and V. A. Artem'ev, *Sov. Phys. JETP* **26**, 1080 (1968).
56. K. Mok, C. Scarlat, G. J. Kovács, L. Li, V. Zviagin, J. McCord, M. Helm, and H. Schmidt, *J. Appl. Phys.* **110**, 123110 (2011).
57. W. Geerts, Y. Suzuki, T. Katayama, K. Tanaka, K. Ando, and S. Yoshida, *Phys. Rev. B* **50**, 12581 (1994).
58. Y. Suzuki, T. Katayama, P. Bruno, S. Yuasa, and E. Tamura, *Phys. Rev. Lett.* **80**, 5200 (1998).